High-lying, non-yrast shell structure in ^{52}Ti

S. Zhu,[1] R. V. F. Janssens,[1] B. Fornal,[2] S. J. Freeman,[3] M. Honma,[4] R. Broda,[2] M. P. Carpenter,[1] A. N. Deacon,[3] E. Jackson,[1,*] B. P. Kay,[3,†] T. Lauritsen,[1] C. J. Lister,[1] P. F. Mantica,[5,6] T. Otsuka,[7,8] D. Seweryniak,[1] J. F. Smith,[3,‡] D. Steppenbeck,[3,§] and X. Wang[1,9,‖]

[1]*Physics Division, Argonne National Laboratory, Argonne, Illinois 60439, USA*
[2]*Institute of Nuclear Physics, Polish Academy of Sciences, PL-31342 Cracow, Poland*
[3]*School of Physics and Astronomy, Schuster Laboratory, University of Manchester, Manchester M13 9PL, United Kingdom*
[4]*Center for Mathematical Sciences, University of Aizu, Tsuruga, Ikki-machi, Aizu-Wakamatsu, Fukushima 965-8580, Japan*
[5]*National Superconducting Cyclotron Laboratory, Michigan State University, East Lansing, Michigan 48824, USA*
[6]*Department of Chemistry, Michigan State University, East Lansing, Michigan 48824, USA*
[7]*Department of Physics, University of Tokyo, Hongo, Tokyo 113-0033, Japan*
[8]*RIKEN, Hirosawa, Wako-shi, Saitama 351-0198, Japan*
[9]*Physics Department, University of Notre Dame, Notre Dame, Indiana 46556, USA*

(Received 3 July 2009; published 31 August 2009)

Gamma rays from ^{52}Ti have been studied with Gammasphere and the Fragment Mass Analyzer using reactions induced by a ^{48}Ca beam on a ^{9}Be target. The data have been used in combination with information from deep-inelastic reactions of ^{48}Ca beams on a thick ^{238}U target at an energy about 25% above the Coulomb barrier. The ^{52}Ti level scheme was expanded considerably, and the lifetimes of some of the identified states were determined for the first time. The excitation of two protons and two neutrons outside the ^{48}Ca core provide new tests of effective interactions in the full pf-shell model space. The positive-parity states in ^{52}Ti were compared to theoretical predictions obtained with the GXPF1A, FPD6, and KB3G effective interactions. The comparisons favor, to a degree, the results computed with the GXPF1A interaction.

DOI: 10.1103/PhysRevC.80.024318 PACS number(s): 21.60.Cs, 23.20.Lv, 25.70.Gh, 25.70.Lm

I. INTRODUCTION

Significant progress has been made recently in exploring the properties of neutron-rich nuclei, in part due to the development of new experimental techniques. From the available data, it has become clear that shell and subshell closures in neutron-rich nuclei may differ significantly from the familiar ones seen in nuclei close to stability. For example, since the onset of a $N = 32$ subshell gap was first proposed from the 2_1^+ energy systematics in neutron-rich Cr isotopes [1], mounting experimental evidence has been accumulating demonstrating the existence of this subshell gap in the Ca, Ti, and Cr isotopic chains [2–5]. This new aspect of shell structure is understood as follows: when protons are removed from the $\pi f_{7/2}$ shell, the neutron $\nu f_{5/2}$ orbital shifts up in energy relative to the $\nu p_{3/2}$ and $\nu p_{1/2}$ levels due to the weakening of the strong attractive monopole interaction between the two f orbitals [2,6]. Many calculations within the full pf-shell model space have been carried out with different effective interactions and most of them reproduce the features of the newly reported Ca, Ti, and Cr yrast level structures [2,7] satisfactorily. The magnitude of the shift in energy of the $\nu f_{5/2}$ orbital is perhaps best described by the GXPF1 Hamiltonian developed by Honma *et al.* [8]. The latter not only provides a good description of the variation in the $E(2_1^+)$ energies in the three isotopic chains near $N = 32$ but also accounts for the behavior of the high-spin states [2,9]. In this context, the absence of the predicted $N = 34$ shell gap between the $\nu p_{1/2}$ and $\nu f_{5/2}$ orbitals in ^{56}Ti was then viewed as somewhat of a surprise [10–12] and as an indication that the interaction did not predict the energy shift of the $\nu f_{5/2}$ orbital with sufficient accuracy. This led to a modified GXPF1 interaction, labeled GXPF1A, with a narrower $\nu p_{1/2} - \nu f_{5/2}$ gap in the effective single-particle energies. With changes to five $T = 1$ matrix elements involving mainly the $\nu p_{1/2}$ and $\nu f_{5/2}$ single-particle orbitals (see Ref. [13] for details), this interaction has provided a consistent description of the known structural properties along the entire chain of neutron-rich Ti isotopes, including ^{55,56}Ti [9,10,12,14]. It also describes the known Ca isotopes [15,16], as well as the low-spin structures of $N \leqslant 35$ Cr isotopes.

It has been speculated that the absence of a $N = 34$ subshell gap in the Ti isotopes is related to the strength of the $\pi f_{7/2} - \nu f_{5/2}$ monopole interaction being such that two $f_{7/2}$ protons are able to bring the $\nu f_{5/2}$ orbital close in energy to the $\nu p_{1/2}$ state. In Ca nuclei, however, the $\pi f_{7/2}$ orbital is empty. Therefore, the $(\nu p_{3/2}, \nu p_{1/2}) - \nu f_{5/2}$ splitting may be sufficient yet to produce a subshell closure at $N = 34$. To verify this hypothesis, the magnitude of the energy separation between the $\nu f_{5/2}$ and $\nu p_{1/2}$ orbitals in Ca isotopes needs to be tracked from experimental data through

*Present address: University of Massachusetts, Lowell, Massachusetts 01854, USA.
†Present address: Physics Division, Argonne National Laboratory, Argonne, Illinois 60439, USA.
‡Present address: School of Engineering and Science, University of Paisley, Paisley PA1 2BE, UK.
§Present address: RIKEN Nishina Center, 2-1 Hirosawa, Wako, Saitama 351-0198, Japan.
‖Present address: Department of Physics, Florida State University, Tallahassee, Florida 32306, USA.

the Ca isotopic chain. Studying the first few excited states in neutron-rich Ca isotopes, such as ^{53}Ca and ^{54}Ca, is one possible approach, because the separation between the first excited states is directly related to the energy gap between these two orbitals. Unfortunately, with the beams presently available, these investigations represent a significant challenge. Another approach involves studying higher-lying states in isotopes closer to stability, although the configurations associated with the levels of interest may be less pure in this case. It was shown that the energy separation between the $p_{3/2}$ and $p_{1/2}$ orbitals in ^{49}Ca is of the order of 2 MeV and is, in fact, very similar to the separation between the $f_{7/2}$ and $p_{3/2}$ states that is responsible for the shell closure at $N = 28$ [17]. With the addition of neutrons, the latter gap remains significant and manifests itself in the structural properties of the neutron-rich $N = 32$ isotones. Recently, the study of the yrast structure of ^{51}Ca has suggested that the $\nu p_{1/2} - \nu f_{5/2}$ energy difference remains such that the 2_1^+ energy in $N = 34$ ^{54}Ca will be as high as ~ 2.5 MeV [15], with the implication that there may still be a $N = 34$ gap in Ca. However, recent measurements by Rejmund *et al.* on ^{50,51,52}Ca [18] led to the conclusion that the $\nu p_{1/2} - \nu f_{5/2}$ energy spacing was only ~ 2.0 MeV, based on comparisons with calculations with a modified KG3B and GXPF1A interactions. As the 2.0-MeV gap would be of the same order as the corresponding separation from ^{49}Ca to ^{52}Ca, these authors concluded that a $N = 34$ gap was unlikely.

As stated above, the configurations of higher excited states are usually more complicated. For example, it has been shown that high-spin states in $^{55-59}$Cr [19–24] and ^{55}V [14] are affected by the presence of the shape-driving $\nu g_{9/2}$ orbital. Hence, the pf shell alone appears to be insufficient for a suitable description of the experimental observations in the high-spin regime, even when the neutron number is around 32.

The aim of the present work is to provide additional experimental information able to test shell-model calculations carried out with a number of Hamiltonians. Here, the spectroscopy of ^{52}Ti is expanded significantly by exploring and focusing on high-lying, non-yrast states. With only two protons and two neutrons outside doubly magic ^{48}Ca, the structure of ^{52}Ti is likely to lend itself to detailed comparisons with calculations limited to the pf model space carried out with different effective interactions such as GXPF1A [13], FPD6 [25], and KB3G [26]. The comparisons between data and calculations will focus not only on energies, spins, and parities but also on lifetimes as the latter provide additional opportunities to probe the many-body wave functions.

The most recent study of the ^{52}Ti yrast structure established states up to 10^+ and an excitation energy of 9088 keV [2]. A thick target was used, and short-lived, non-yrast states were not observed as a result. Earlier, a two-neutron transfer reaction ^{50}Ti$(t, p\gamma)^{52}$Ti [27] and a β-decay measurement of ^{52}Sc into ^{52}Ti [28] had been performed to provide information on states with excitation energies exceeding 5 MeV but with spins of $4\hbar$ or less. The lifetimes of several states have been determined with the Doppler shift attenuation method (DSAM) in the ^{50}Ti$(t, p\gamma)^{52}$Ti study [27]. Since then, two additional measurements have been performed to deduce the lifetime of the 2_1^+ state. The absolute $B(E2; 0^+ \rightarrow 2_1^+)$ transition rate was determined with intermediate-energy Coulomb excitation [3], and a lifetime value of 3.9(4) *ps* was deduced. A value of 5.2(2) *ps* is reported in Ref. [29] from a DSAM experiment with the ^{12}C(^{48}Ca,^{8}Be) reaction where a lifetime of 4.8(6) *ps* for the 4_1^+ state was also obtained. In addition, the g factors of the 2_1^+ and 4_1^+ states were determined for the first time [29].

The present work combines data using a fusion-evaporation reaction producing ^{52}Ti with information derived from β decay into the same nucleus following a deep-inelastic reaction. Thirty-two states have been observed in this study, 14 of which had not been reported previously. Most of the newly established states are located at excitation energies between 4 and 7 MeV and have spins between $4\hbar$ and $10\hbar$. Lifetimes of nine states were measured using the DSAM method. Comparisons between the data and shell-model calculations favor, to a degree, the results obtained with the GXPF1A effective interaction over those derived with the FPD6 and KB3G Hamiltonians.

II. EXPERIMENTAL PROCEDURE

With proper beam-target combinations, heavy-ion induced fusion-evaporation reactions have proved suitable to populate high-spin states in neutron-rich nuclei located fairly close to stability. For example, the technique was exploited in studies of the neutron-rich Cr isotopes [19–23]. There are, however, limitations to the approach as illustrated by the fact that, in Ref. [14], the ^{55}Ti nucleus could not be studied with the ^{48}Ca+^{9}Be reaction. Presumably, the cross section for the $2p$ channel is smaller in this instance than it was in the successful Cr studies of Refs. [19,20,23]. This may be due to the presence of strong, competing incomplete fusion reactions. The latter favor the production of ^{52}Ti as shown below.

A 172-MeV ^{48}Ca beam, delivered by the Argonne Tandem-Linac Accelerator System (ATLAS), was used to bombard a self-supporting ^{9}Be target of 1.90(1)-mg/cm^2 thickness, determined by measuring the energy loss of 5812-keV α particles. The target was oriented at an angle of 62.5° with respect to the beam direction. Prompt γ rays were detected with the Gammasphere array [30] consisting of 101 Compton-suppressed HPGe detectors. Reaction products recoiling from the target were separated from the primary beam and dispersed in terms of their mass-to-charge ratio (A/Q) by the Fragment Mass Analyzer (FMA) [31]. At the focal plane of the instrument, a parallel-grid avalanche counter (PGAC) measured the horizontal and vertical positions of the recoils and provided timing signals. The residues were subsequently fully stopped in an ionization chamber with three segmented anodes [32], and their energy-loss characteristics were recorded. To trigger the data acquisition, one prompt γ ray had to be detected by Gammasphere in coincidence with a residue with $A/Q = 55/18$, as selected by slits positioned in front of the FMA focal plane. Because of mass-to-charge ratio ambiguities, residues with $A/Q = 52/17$ were detected at the focal plane as well. A total of 1.4×10^8 events were collected in this way.

Isotopic selection of the residues was achieved by analyzing the energy loss in the three segments of the ionization chamber.

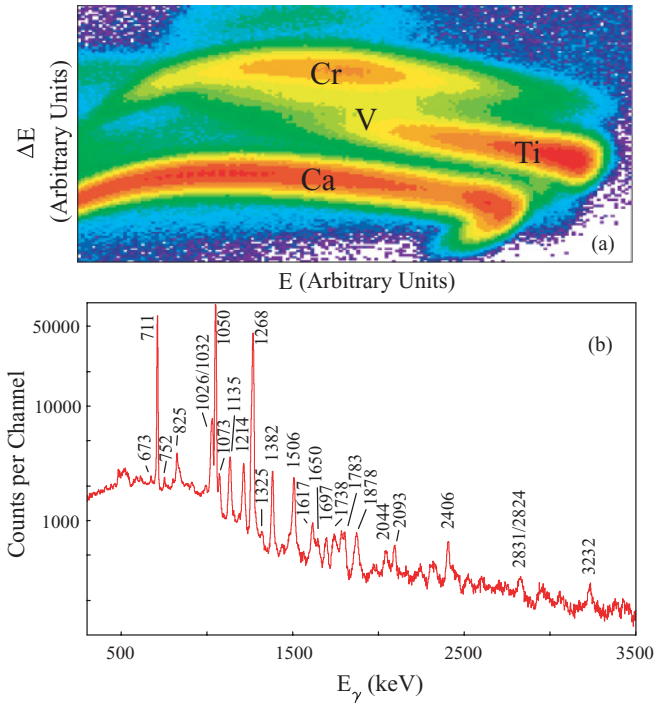

FIG. 1. (Color online) (a) Two-dimensional plot of E vs. ΔE. The residues with different Z values are well separated. (b) Spectrum of γ rays in coincidence with ^{52}Ti residues selected by gating on the relevant part of the E vs. ΔE plot.

This is illustrated in Fig. 1(a) where the energy loss ΔE in the first two segments is plotted against the total energy loss E and the Ti, V, and Cr isotopes are clearly separated. The γ rays in coincidence with the ^{52}Ti residues can be found in Fig. 1(b), and these γ rays were organized into a prompt $\gamma\gamma$ coincidence matrix. It can be seen that, except for the strong 1050-, 1268-, and 711-keV yrast transitions [2], the remaining γ rays are much weaker. In addition, as indicated in Fig. 2, the time of flight through the FMA for the recoils corresponding to ^{52}Ti residues is distinctly shorter than that for the other products.

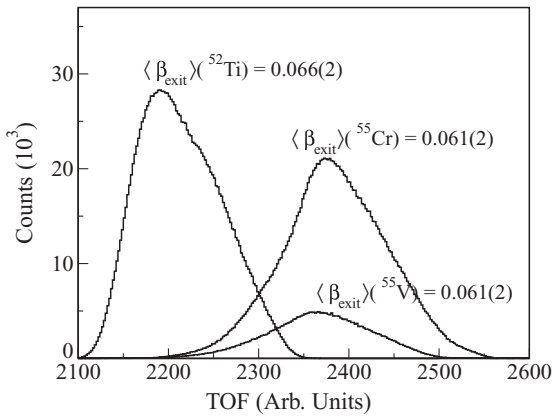

FIG. 2. The distributions of time of flight between the target and the FMA focal plane for ^{52}Ti, ^{55}V, and ^{55}Cr residues. The $\langle\beta\rangle$ values obtained from the calibrated β and time-of-flight relation are indicated in the figure also.

As alluded to above, this can be accounted for by postulating that the reaction producing ^{52}Ti is not a fusion-evaporation one but occurs with much larger Q values. By analyzing the Doppler effects experienced by de-excitation γ rays detected in the 16 rings of Gammasphere, the recoil velocities in units of the speed-of-light for ^{52}Ti and ^{55}Cr recoils were independently determined to be $\beta = 0.0662(1)$ and $0.0611(1)$, respectively. These recoil velocities translate into respective kinetic energies of 107.7(3) and 97.0(3) MeV indicating a 10.7 MeV difference in Q value between the reactions producing the two residues, consistent with an incomplete-fusion mechanism.

In previous studies of nuclei in this region [9,14,15,23], an experiment with a 330-MeV ^{48}Ca beam bombarding a 50 mg/cm^2-thick ^{238}U target was carried out, where the beam was pulsed with a 410-ns repetition rate, each beam pulse being $\sim$0.3 ns wide. An event was accepted when three or more of the 101 Compton-suppressed HPGe detectors fired within 1 μs. Prompt γ rays can be separated from those detected between beam bursts by using the time information from the individual detectors. A so-called delayed $\gamma\gamma\gamma$ coincidence cube was created containing γ rays observed in an interval of $\sim$ 40–350 ns after the beam burst, with the additional requirement that the three signals were within $\sim$40 ns of each other.

The multipolarities of prompt transitions were assigned based on the measured angular distributions expressed as a ratio of the efficiency-corrected intensities measured in detectors perpendicular and along the beam axis. The former includes HPGe detectors in rings located at 79°, 81°, 90°, 99°, and 101°, while the latter consider counters in the 32°, 37°, 143°, 148°, and 163° rings. Gamma rays with a measured ratio larger than one are consistent with $\Delta I = \pm 2$ or $\Delta I = 0$ transitions. For dipole transitions, the ratio is smaller than one. These ratios alone are often not sufficient to assign spin and parity to a given state. Additional information and arguments can be used based, for example, on intensity (prompt and delayed) or the presence/absence in the spectra following β decay.

Because the time-of-flight parameter of the recoils is directly related to their velocity, it is possible to apply a Doppler-shift correction to all the γ rays on an event-by-event basis rather than to use an average velocity derived from reaction kinematics. The three strong γ rays in ^{52}Ti, evident in Fig. 1(b), were sufficiently intense to establish the relationship between time of flight and velocity. Using this relation, the remainder of the γ rays will be corrected properly for the Doppler shift if the associated lifetimes are such that emission occurs after the recoils have left the target. Inspection of the spectra indicated, however, that the corrections for some of the γ rays were not optimized, i.e., the energies of these γ rays, as measured in the forward rings, were still too high after the correction, and were too low in the backward rings. This is an indication that the lifetimes of the de-exciting states are sufficiently short that emission occurs while the recoils are being slowed down in the target.

The mean velocities of the de-exciting states during the slowing down process can be expressed as

$$\langle v\rangle = \frac{\int N(t)v(t)dt}{\int N(t)dt} \qquad (1)$$

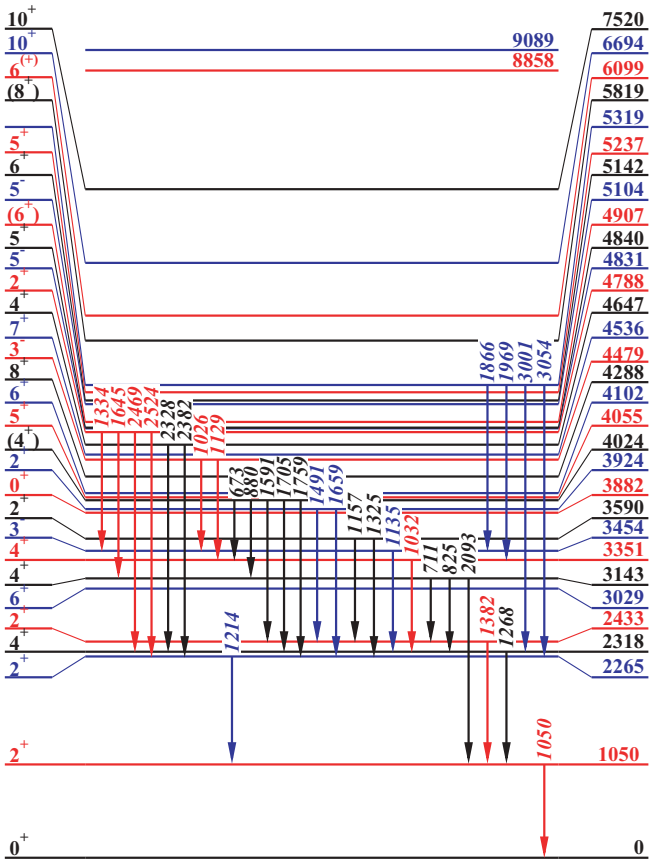

FIG. 3. (Color online) Partial level scheme of ^{52}Ti proposed by this work. Only transitions observed in the β-decay part of this work are presented here. Colors are alternating to ease the reading of the level sequence.

from which the apparent lifetime of the state (i.e., level plus side-feeding lifetime) is derived as

$$\tau(\text{fs}) = \frac{m(\text{MeV})}{dE/dx(\text{MeV}/\mu\text{m})} \frac{\beta_0 - \langle\beta\rangle}{c(\mu\text{m/fs})} \qquad (2)$$

assuming that the stopping power dE/dx is constant within the target, an assumption valid here in view of the target thickness. In Eq. (1), $\langle v\rangle$ is the mean velocity and $v(t)$ and $N(t)$ are the velocity and number of de-exciting states at time t. In Eq. (2), τ is the mean lifetime of the state in fs, m is the mass of the recoiling nuclei in MeV, and c is the speed of light in μm/fs. The dE/dx energy loss can be calculated with the SRIM package [33]. The validity of this approach in this specific application was checked for the case of ^{55}Cr, where the recoiling energy at the exit of the target computed with SRIM agrees to within 0.5% with the measured value. In the present analysis, a SRIM stopping power of $dE/dx = 0.6039(3)$ MeV/μm was adopted taking into account the effective target thickness and beam energy. The initial recoil velocity is computed to be $\beta_0 = 0.0762(1)$ [with $\beta_{\text{exit}} = 0.0662(1)$ at the exit of the target]. Because of the coupling of the FMA with Gammasphere, the recoil direction is well defined by the small aperture at the FMA entrance [31], implying that the impact of angle straggling on the mean velocities is minimized. In addition, the high recoil velocity limits the stopping mechanism to electronic stopping mainly, which is well understood. Two different methods were applied to obtain the effective $\langle\beta\rangle$ values for the individual γ-ray transitions. For the γ rays with sufficient intensity, the $\langle\beta\rangle$ values were measured by fitting the transition energies measured in each ring of Gammasphere. For γ rays with lower statistics, the appropriate $\langle\beta\rangle$ value was derived in a procedure where the minimum value of the width of the photopeak (FWHM) was obtained by variation of the Doppler correction.

III. RESULTS

The observed γ-ray transitions were placed into the ^{52}Ti level scheme presented in Figs. 3 and 4, by examining background-subtracted, gated coincidence spectra obtained from the prompt $\gamma\gamma$ matrix and delayed $\gamma\gamma\gamma$ cube described above. The decay pattern of the level scheme was split into two figures. All the γ rays observed in the delayed cube (i.e., from β decay) are shown in Fig. 3, while those observed only in the prompt matrix are displayed in Fig. 4. The three panels in Fig. 5 provide spectra double-gated on the three lowest branches in β decay. The γ rays in coincidence with these branches are identified. Most of the states known from the previous β-decay study [28] were confirmed, except the 4078- and 4286-keV

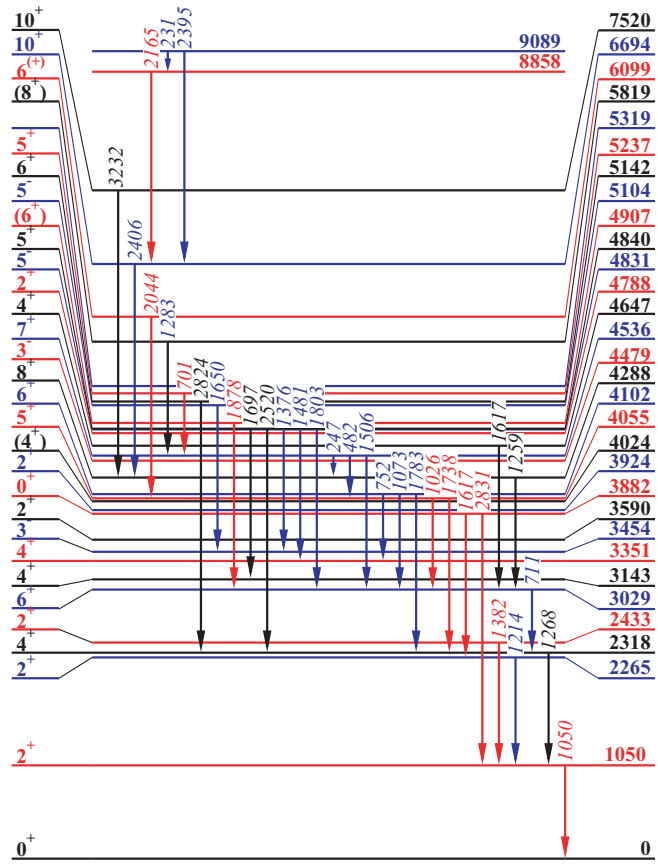

FIG. 4. (Color online) Partial level scheme of ^{52}Ti proposed by this work. Only prompt γ rays are given in this figure. Colors are alternating to ease the reading of the level sequence.

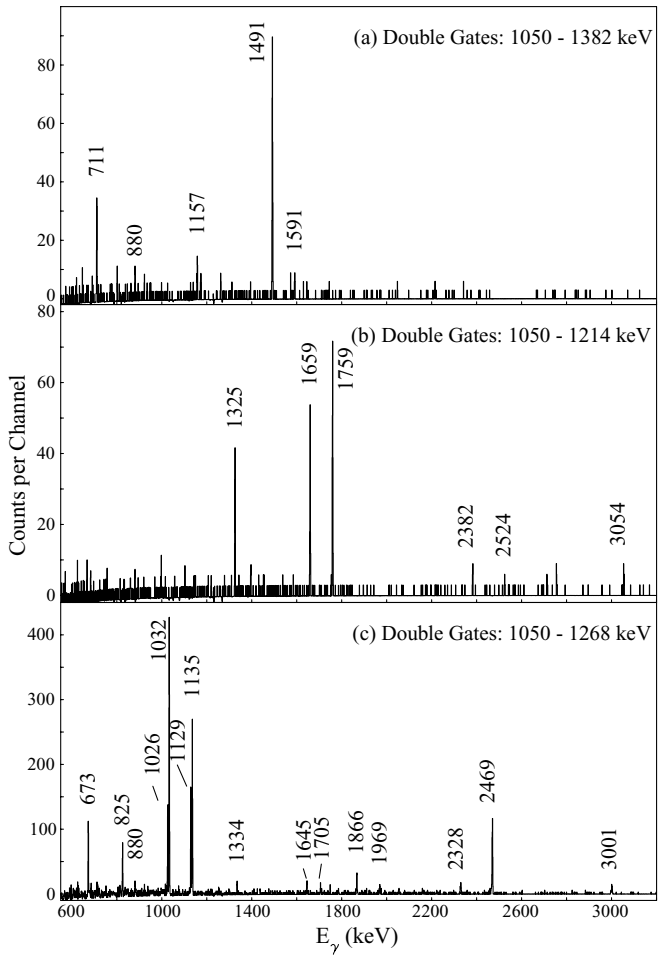

FIG. 5. Out-of-beam coincidence spectra for ^{52}Ti showing the γ rays observed in β decay in the present work.

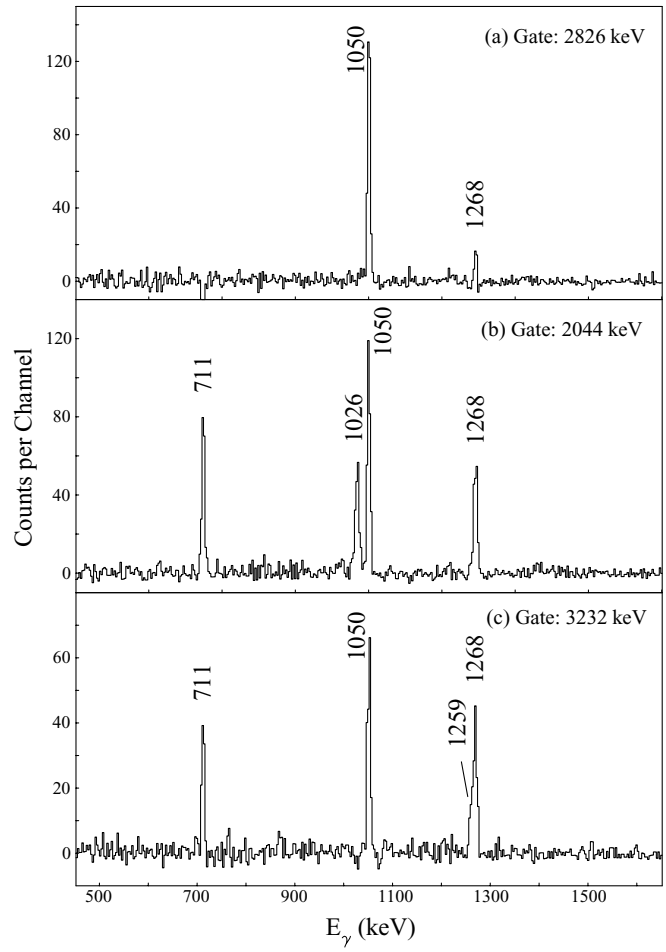

FIG. 6. Representative coincidence γ-ray spectra gated with the specified transitions in ^{52}Ti as observed in the ^{48}Ca+^{9}Be reaction.

levels. In addition, two levels at 4647 and 5319 keV were added to the decay scheme. As illustrated by the coincidence spectra of Fig. 5, four weak transitions with energies 1866, 1969, 3001, and 3054 keV have been uncovered, and they were placed as linking the 5319-keV level with the 3^- ($E_{\text{level}} = 3454$ keV), 4^+ (3143 keV), 4^+ (2318 keV), and 2^+ (2265 keV) states, respectively. It is noted that the 1969-keV γ ray was assigned as de-exciting the 4286-keV level in the previous β-decay study, but based on its coincidence relationship with the 1032-keV transition, it is revised and placed as the link between the 5319- and 3351-keV levels. The 4647-keV level was established in the same manner with the observation of the weak 2382- and 2328-keV γ rays.

As stated above, in the ^{48}Ca+^{9}Be experiment, where high-spin, non-yrast states in ^{52}Ti were populated, the optimum energy resolution in the γ-ray spectra was achieved by performing the Doppler correction on an event-by-event basis using the calibrated time-of-flight parameter. The quality of the data is demonstrated in Fig. 1(b). Even though the intensities for most of the γ rays in the figure are much weaker than the three transitions in the main cascade, they are still sufficient for an in-depth $\gamma\gamma$ coincidence analysis. Using the β-decay scheme as a starting point, the coincidence relationships between the γ transitions were established. For instance, in Fig. 6, spectra generated by placing gates on the three weak transitions with energy 2826,[1] 2044, and 3232 keV revealed that they decay through different pathways. The 2044-keV γ ray is in coincidence with the 1026-keV transition, and the 1259-keV peak next to the 1268-keV line is absent, while in the spectrum gated with the 3232-keV γ ray, the cascade with 1050-, 1268-, 711-, and 1259-keV transitions is prominent. Therefore, the 2044-keV transition was proposed as de-exciting from the 6099-keV level to the 4055-keV state, and the 3232-keV transition depopulates the 7520-keV state (Fig. 4). By gating on the 2826-keV γ ray, two peaks at 1050 and 1268 keV are seen, but with an intensity ratio that differs from that in the 2044- and 3232-keV gated spectra. The intensity of the 1050-keV line is larger than expected when comparing to the 1268-keV yield, suggesting that the 2826-keV γ ray is a doublet, with one component feeding 1050-keV level directly, and the other decaying to the 2318-keV state. For high-energy γ rays, the Doppler effects are large, and the detection efficiencies are low. Therefore, it is

[1]The 2826-keV energy quoted here is the centroid of a doublet. The actual energies of the two transitions are discussed further down in this section.

TABLE I. Levels identified in ^{52}Ti together with lifetimes, transition energies, γ-ray intensities measured in-beam and angular ratios as defined in the text.

E_{level} (keV)	J^{π}	Lifetime (fs)	E_{γ} (keV)	I_{γ} (%)	Angular ratio
1050.2(1)	2^+		1050.2(1)	100(5)	1.20(1)
2264.7(1)	2^+	56(8)	1214.4(1)	5.6(3)	1.33(4)
2318.4(1)	4^+		1268.2(1)	75(4)	1.29(1)
2432.5(1)	2^+	171(11)	1382.3(1)	5.4(3)	1.21(6)
3029.3(2)	6^+		710.9(1)	46(2)	1.26(1)
3143.2(1)	4^+	139(27)	2093.0(1)	1.2(2)	1.4(1)
			824.9(1)	2.9(2)	1.7(1)
			710.6(1)	1.2(2)	
3350.8(1)	4^+		1032.3(1)	11(2)	1.8(2)
3453.7(1)	3^-	59(8)	1135.4(1)	7.0(3)	0.75(8)
3589.5(1)	2^+		1324.7(1)	0.6(1)	1.4(2)
			1157.1(1)	0.20(3)	
3881.7(1)	0^+		2831(3)	0.6(1)	
			1617(1)	0.9(1)	1.1(2)
3923.7(1)	2^+		1659.0(1)		
			1491.2(1)	0.42(7)	
4023.5(1)	(4^+)		1758.8(1)	0.28(5)	1.2(1)
			1705.2(1)		
			1590.5(3)		
			880.4(2)		
			672.6(1)	0.6(1)	
4054.7(8)	5^+		1738(2)	1.4(2)	0.80(8)
			1026(1)	0.8(2)	
4102.4(7)	6^+		1783(2)	1.5(2)	
			1073(1)	1.9(2)	1.2(1)
			752(1)	1.2(2)	
4287.9(2)	8^+		1258.6(1)	11.8(6)	1.32(5)
4479.4(2)	3^-		1128.6(1)	0.8(2)	
			1025.7(1)	4.5(3)	1.42(8)
4535.6(7)	7^+	123(22)	1506(1)	6.0(3)	0.85(4)
			482(1)	0.05(1)	
			247(1)	0.6(1)	
4646.8(2)	4^+		2382.1(3)		
			2328.3(3)		
			1617(1)	0.53(6)	1.5(2)
4787.8(2)	2^+		2524.1(5)		
			2469.2(1)		
			1644.5(3)		
			1334.1(1)		
4831.3(6)	5^-		1803(1)	0.97(9)	0.8(1)
			1481(1)	0.6(2)	0.7(2)
			1376(1)	0.30(6)	
4840(1)	5^+	86(26)	2520(3)	0.08(2)	
			1697(1)	0.33(6)	0.74(9)
4907(1)	(6^+)	54(19)	1878(1)	2.9(2)	1.4(1)
5104(1)	5^-		1650(1)	0.52(8)	1.7(4)
5142(6)	6^+		2824(6)	0.4(1)	1.30(18)
5237(1)	5^+		701(1)	1.2(3)	1.2(1)
5319.4(2)			3054.0(5)		
			3001.1(3)		
			1968.5(2)		
			1865.8(2)		
5819(1)	(8^+)		1283(1)	1.4(3)	0.7(2)
6099(2)	$6^{(+)}$	86(26)	2044(2)	1.3(2)	0.8(1)
6694(2)	10^+		2405.6(1)	1.8(2)	1.2(1)
7520(3)	10^+	59(26)	3232(3)	0.9(1)	1.3(1)
8858.0(2)			2164.6(1)	0.43(8)	
9089.2(2)			2395.3(1)	0.11(5)	
			231.4(1)	0.06(3)	

difficult to resolve the two components of this γ ray directly. However, the energy of one component of the doublet could be determined as 2831 keV because the excitation energy of the depopulating state (3882 keV) is also determined by the 1617-keV transition linking it to the 2265-keV level. With the energy of one component fixed, the energy of the other was fitted as 2824 keV, establishing a 6^+ level at 5142 keV.

An extended ^{52}Ti level scheme was proposed by gating on the rest of the observed γ rays in the prompt matrix through the same procedure. Table I summarizes the experimental information on the γ-ray transitions and energy levels in ^{52}Ti. Only the relative intensities from the in-beam measurement are listed in the table. The spin-parity assignments for the states at 1050, 2265, 2318, 2433, 3351, 3454, 3590, 3924, and 4788 keV were adopted on the basis of the ^{50}Ti(t, p) measurements of Ref. [34]. The multipolarities of the transitions among these states reported here are consistent with the respective assignments. The 3029-, 4288-, and 6694-keV states were assigned 6^+, 8^+, and 10^+ quantum numbers based on the measured angular ratios as well as on yrast-feeding arguments. For many other levels in Figs. 3 and 4, however, β-decay information from the delayed cube was instrumental in restricting spin-parity assignments as illustrated below, given that the ground state of the parent nucleus, ^{52}Sc, is $3^{(+)}$ [34].

For example, considering the 3882-keV level, the 1617-keV transition was found to be in coincidence with the 1050- and 1214-keV γ rays in the in-beam experiment but absent in the spectrum generated by double-gating on the 1050- and 1214-keV γ rays in the delayed cube. Furthermore, its angular ratio was measured to be 1.1(2), indicating an isotropic distribution. These observations restrict the spin and parity of the 3882-keV state to either 0^+ or 1^+. With an 1^+ assignment, a strong 3882-keV transition would be expected as a link between the level of interest and the ground state, in competition with the 2831- and 1617-keV γ rays. However, such a transition is absent for a 0^+ state, in agreement with the experimental observations. This 0^+ assignment also accounts for the isotropy of the 1617-keV γ ray.

The J^{π} values of the 3143- and 4840-keV states were determined as follows. The spin difference between the two levels is restricted to $\pm 1\hbar$, based on the angular ratio (<1) of the 1697-keV transition. In addition, the former state is populated in β decay while the latter was only observed in-beam, and these observations are consistent with the proposed 4^+ and 5^+ assignments.

The de-excitation of the 4055-keV level toward the 4_1^+ and 6_1^+ states, but not to the 3^- state, is solely observed in the in-beam spectra. This observation, combined with the dipole

TABLE II. Detailed comparison between the experiment and shell-model calculations with GXPF1A, FPD6, and KB3G effective interactions for level energies and associated lifetimes (where available).

J^π	Experiment		GXPF1A		FPD6		KB3G	
	Energy (keV)	τ (fs)	Energy (keV)	τ (fs)	Energy (keV)	τ (fs)	Energy (keV)	τ (fs)
0_1^+	0		0		0		0	
2_1^+	1050.2(1)	4.9(5) *ps*[a]	1106	5.1 *ps*	1236	2.5 *ps*	1069	6.2 *ps*
2_2^+	2264.7(1)	56(8)	2071	49	2405	36	2065	62
4_1^+	2318.4(1)	4.8(6) *ps*[b]	2251	3.8 *ps*	2294	5.1 *ps*	2356	2.1 *ps*
2_3^+	2432.5(1)	171(11)	2552	90	2751	513	2442	46
6_1^+	3029.3(2)	25(4) *ps*[c]	2932	66.6 *ps*	3178	18.1 *ps*	3048	68.4 *ps*
4_2^+	3143.2(1)	139(27)	3255	49	3100	66	3274	30
4_3^+	3350.8(1)		3383		3892		3550	
2_4^+	3589.5(1)	<62[c]	3708	18	3264	90	3551	59
0_2^+	3881.7(1)		3839		2871		3681	
2_5^+	3923.7(1)		3951		3995		3851	
(4_4^+)	4023.5(1)		3900		4430		4051	
5_1^+	4054.7(8)		3953		4285		4194	
6_2^+	4102.4(7)		3969		4570		4286	
8_1^+	4287.9(2)		4296		4832		4416	
7_1^+	4535.6(7)	123(22)	4506	77	5129	34	4749	44
4_5^+	4646.8(2)		4492		4684		4601	
5_2^+	4840(1)	86(26)	4643	21	4706	203	4695	32
(6_3^+)	4907(1)	54(19)	4902	31	4755	198	4954	27
6_4^+	5142(3)		5371		5508		5372	
5_3^+	5237(1)		4926		5041		4976	
(8_2^+)	5819(2)		5927		5708		5757	
$6_5^{(+)}$	6099(1)	86(26)	5710	42	6075	341	5925	84
10_1^+	6694(2)		6548		6165		6428	
10_2^+	7520(3)	59(26)	8176	28	8855	81	8651	30

[a]Weighted average of 3.9(4) *ps* [3] and 5.2(2) *ps* [29].
[b]From Ref. [29].
[c]From Ref. [34].

character of the 1738-keV γ ray, leads to the proposed 5^+ assignment. The 6^+ assignment for the 5142-keV level follows from the absence of the 2824-keV transition in β decay and its quadrupole character in the in-beam data. The level at 4536 keV decays toward three states with respective spins and parity 6^+, 5^+, and 8^+ through the 1506-, 482-, and 247-keV γ rays. This pattern, combined with the dipole character of the 1506-keV γ ray, justifies the 7^+ assignment to the 4536-keV state. The 6099-keV level depopulates directly to the 5^+ state at 4055 keV via a 2044-keV dipole transition that is absent from the β-decay spectra, and was therefore assigned spin 6.

The proposed 10^+ spin and parity for the 7520-keV level is based on the quadrupole character of the 3232-keV γ ray and the supporting consideration that an 8^+ assignment would result in the feeding of a level more than 3 MeV above the yrast line, a feature deemed unlikely for the reaction used here. The 4102-keV level is proposed as the second 6^+ level, because it is de-excited by 1783- and 752-keV transitions leading to the second and third 4^+ states, respectively, and a 1073-keV transition to the first 6^+ level that has an angular-distribution ratio larger than unity. Similarly, the 5^- assignment to the 4831-keV state follows from the observation of the 1803- and 1481-keV dipole transitions feeding the 6_1^+ and 4_3^+ levels as well as the presence of a 1376-keV γ ray reaching the 3^- state at 3454 keV. The newly discovered level at 4647 keV was observed to be linked to the 2_2^+, 4_1^+, 6_1^+ states through the 2382-, 2328-, and 1617-keV transitions, restricting possible spin options to 2, 3, and 4. The proposed 4^+ assignment follows from the quadrupole character of the 1617-keV γ ray. Both the 4479- and 5104-keV states decay toward the 3^- level at 3454 keV through transitions with angular ratios larger than 1.0. The former is also seen in β decay, resulting in a 3^- assignment, while the latter is proposed as a 5^- level.

Some of the states reported here could not be given rigorous spin-parity assignments based solely on experimental considerations. In such instances, the results of the shell-model calculations were used, as discussed in the next section.

The lifetimes of a number of states are also given in Table I. As stated in the Introduction, several lifetime measurements have been reported for the 2_1^+ level and the value quoted in Table II is a weighted average of data from Refs. [3] and [29]. The latter work also provide the lifetime of the 4_1^+ state listed

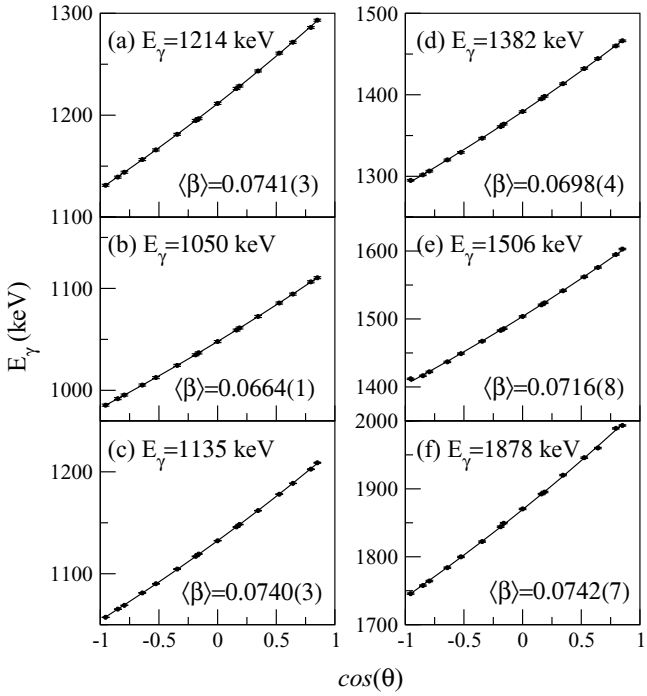

FIG. 7. Mean β values obtained from the fit of the γ-ray energies measured in Gammasphere at different angles relative to the beam direction. The 1050-keV γ ray corresponding to the $2_1^+ \rightarrow 0^+$ transition is emitted after ^{52}Ti has left the target because of the intrinsic lifetime of the 2_1^+ state (see Table II). Hence, the measured β value represents the recoil velocity through the FMA.

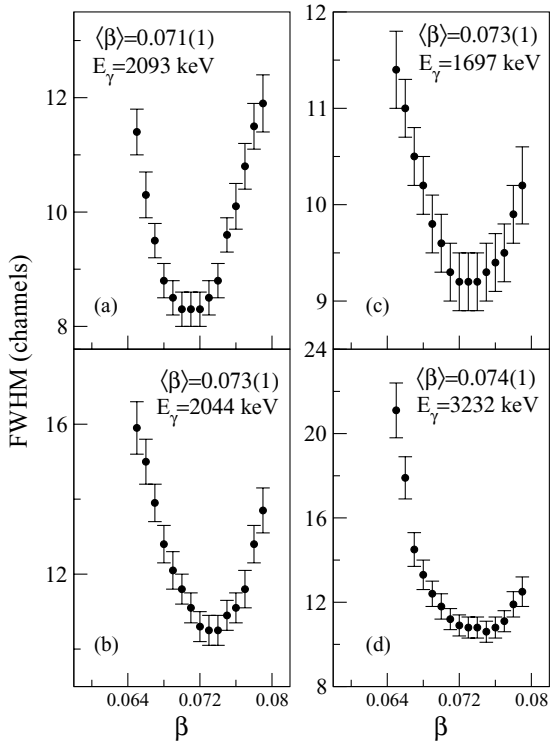

FIG. 8. Mean β values obtained by searching for the optimum FWHM values by varying the recoil velocity β; see text for details.

in Table II. Here, new information was derived for nine states with the methods described in Sec. II. For the 1050-, 1135-, 1214-, 1382-, 1506-, and 1878-keV γ rays, the average recoil velocity $\langle\beta\rangle$ was derived from the fit of the measured energies in the individual rings of Gammasphere with the equation $E(\theta) = E_0 \frac{\sqrt{1-\beta^2}}{1-\beta\cos\theta}$ (method 1), as illustrated in Fig. 7. For four additional transitions (1697, 2044, 2093, and 3232 keV) the second method of Sec. II was used, i.e., the peak widths [full width at half maximum (FWHM)] were minimized by varying the recoil velocity as shown in Fig. 8. In the discussion below, the extracted lifetimes will be considered to be the intrinsic state lifetimes, as feeding transitions from high-lying states were found to be of small intensities.

IV. DISCUSSION

High-spin, non-yrast states can be useful in probing structural changes as a function of spin and excitation energy by comparing the experimental information with the results of shell-model calculations. The shell-model description of ^{52}Ti can, in principle, be fairly simple under the assumption of a closed ^{48}Ca core. In this experiment, the detailed information on high-lying, non-yrast states in ^{52}Ti is compared in Table II with results from full pf shell-model calculations carried out with the commonly used effective interactions GXPF1A [13], FPD6 [25], and KB3G [26]. At most five states for each spin and parity are included in the comparisons so that the experimental uncertainty associated with very weak γ rays located far above the yrast line can be avoided. These effective interactions have all proven to provide consistent descriptions of nuclei close to stability in this mass region. For neutron-rich nuclei, they were found often to predict different sequences of orbitals with respect to the Fermi surface and different single-particle energies. The effective single-particle energies for the $p_{3/2}$, $p_{1/2}$, and $f_{5/2}$ neutron orbitals, with respect to the $f_{7/2}$ neutron orbital, calculated with the three effective interactions are compared for the Ca and Ti isotopic chains in Fig. 9. Marked differences between calculations with these

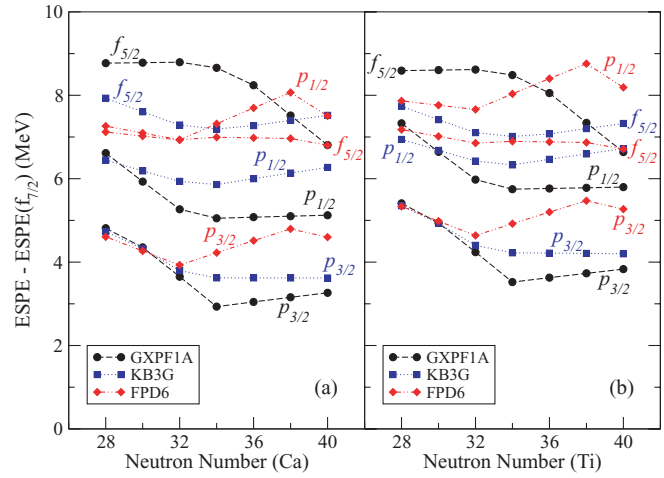

FIG. 9. (Color online) Effective single-particle energies of $\nu p_{3/2}$, $\nu p_{1/2}$, and $\nu f_{5/2}$ orbitals relative to $\nu f_{7/2}$ orbital for calcium and titanium isotopes from $N = 28$ to $N = 40$.

interactions are rather striking. These differences should also be reflected in the description of the high-lying, non-yrast states in ^{52}Ti.

As already alluded to above, for some states observed in the present work, spin and parity assignments could not be proposed on the basis of the available experimental information. Quantum numbers were tentatively assigned here on the basis of the calculations. Thus, the spin and parity of the 4024-, 4907-, 5819-, and 6099-keV levels are tentatively assigned 4^+, 6^+, 8^+, and 6^+, respectively, as calculations with the three interactions provide essentially the same quantitative agreement with the data. In the computation of the lifetimes from the calculated $B(E2)$ transition probabilities, the values of the proton and neutron effective charges were adopted as $e_p = 1.15e$ and $e_n = 0.8e$, respectively. This procedure was first used in Ref. [3] and is based on isospin conservation arguments developed recently in conjunction with lifetime measurements on analog states in $A = 51$, $T_z = \pm 1/2$ mirror nuclei [35]. For the computation of the lifetimes of states de-exciting via $M1$ transitions, the effective g factors used are $g_{lp} = 1.1$, $g_{ln} = -0.1$, and $g_s = 0.9 g_s$(free). These values were adopted based on fits of known magnetic moments of nuclei in the region with the GXPF1 effective interaction [36].

Because the shell-model calculations within the full pf shell do not produce negative-parity states in ^{52}Ti, and because these states can be understood as resulting from coupling to the 3^- state, they are excluded from the following comparisons with the shell-model calculations.

For the states with positive parity, each of the three interactions predicts the excitation energies within an rms deviation better than 500 keV. Quantitatively, results of calculations with the GXPF1A interaction seem somewhat more accurate with an rms deviation of 201 keV, followed by those with the KB3G Hamiltonian with a 273-keV rms value, and the FPD6 interaction that results in an rms value of 456 keV. As a result, this article focuses mostly on comparisons based on the GXPF1A Hamiltonian although, when significant differences with calculations using the other interactions occur, these will be discussed as well.

In the calculated spectrum with the GXPF1A interaction, the $\pi f_{7/2}^2 \nu p_{3/2}^2$ configuration is the leading one, with a $\geqslant 50\%$ contribution in the wave functions of the 0_1^+, 2_1^+, 2_2^+, 4_1^+, 6_1^+, 4_2^+, 0_2^+, 5_1^+, 6_2^+, 8_1^+, and 7_1^+ states, and the corresponding excitation energies are calculated with an rms deviation of only 99 keV. This value is also the smallest among those obtained for this set of states with all interactions. However, it is noteworthy that the FPD6 Hamiltonian reproduces the 4_1^+ energy within 24 keV only, but it describes this state with two dominant configurations: 28% $\pi f_{7/2}^2 \nu p_{3/2}^1 f_{5/2}^1$ and 19% $\pi f_{7/2}^2 \nu p_{3/2}^2$. This is a reflection of the lower energy location of the $\nu f_{5/2}$ orbital as compared to that adopted in the GXPF1A case. In addition, as shown in Table II, the experimental lifetime of the 4_1^+ state was found to be in somewhat better agreement with the FPD6 prediction. On the basis of this single observation alone, one might be tempted to conclude that the FPD6 Hamiltonian provides a better description of the relative location of the $\nu f_{5/2}$ orbital, but, in fact, the situation is reversed when the remainder of the experimental data is taken into account. It was also noticed that the FPD6 interaction predicts a sizable admixture of the $\pi f_{7/2}^2 \nu f_{5/2}^2$ configuration (9%) in the ground-state wave function, with the main $\pi f_{7/2}^2 \nu p_{3/2}^2$ component taking only a 47% weight instead of the 63% value given by the GXPF1A Hamiltonian. As a result, the FPD6 interaction overpredicts the energies of the 2_1^+, 2_2^+, 6_1^+, 4_3^+, 8_1^+, 7_1^+, and 6_4^+ levels, which are associated closely with the $\pi f_{7/2}^2 \nu p_{3/2}^2$ configuration (weight $\geqslant 40\%$) by 141 keV at the minimum and by as much as 594 keV, leading to an rms value of 406 keV for the total set of these states. The second 0_2^+ state is dominated by the $\pi f_{7/2}^2 \nu p_{3/2}^2$ configuration (48%) according to the GXPF1A calculations, while its wave function is more mixed (38% $\pi f_{7/2}^2 \nu f_{5/2}^2$ and 15% $\pi f_{7/2}^2 \nu p_{3/2}^2$) in the FPD6 case. Here again, the GXPF1A calculation comes within only 52 keV of the data while the FPD6 state is 1010 keV lower. This can be viewed as another indication that the adopted energy spacing between the $\nu p_{3/2}$ and $\nu f_{5/2}$ orbitals assumed by the GXPF1A Hamiltonian results in a better agreement between the shell-model results and the experimental data. One additional observation reinforcing the adequacy of the GXPF1A interaction with respect to the location of the $\nu f_{5/2}$ orbital is related to the 10_1^+ state. Its wave function is dominated (74%) by the $\pi f_{7/2}^2 \nu p_{3/2}^1 f_{5/2}^1$ configuration in the GXPF1A calculations, which reproduce the energy of this state within 143 keV, a number to be compared with 526 keV for the FPD6 case. The relative success of the GXPF1A interaction can also be seen in its ability to reproduce the lifetimes of the relevant states. As indicated in Table II, most of the lifetimes predicted by the FPD6 Hamiltonian deviate significantly from the measured values, which in turn agree better with the calculations using the GXPF1A and KB3G interactions.

The wave function of the 10_1^+ state given by the KB3G effective interaction is similar to that derived with the GXPF1A one, but with an excitation energy of 6428 keV. This reflects the general trend that the behavior of the $\nu f_{5/2}$ orbital in the shell-model calculations (Fig. 9) with the KB3G effective interaction, while not as good as that with the GXPF1A Hamiltonian, appears to be more accurate than that computed in the FPD6 case.

It was hoped that additional information on the relative location in excitation energy of the $\nu p_{1/2}$ and $\nu f_{5/2}$ orbitals might come from further comparisons between calculations with the KB3G and GXPF1A interactions. States with dominant $\pi f_{7/2}^2 \nu p_{3/2} f_{5/2}$ and $\pi f_{7/2}^2 \nu p_{3/2} p_{1/2}$ configurations can be identified for both cases and some differences can be noted. For example, the 2_4^+ state computed with the KB3G Hamiltonian has a strong $\pi f_{7/2}^2 \nu p_{3/2} f_{5/2}$ component in its wave function, while the $\pi f_{7/2}^2 \nu p_{3/2} p_{1/2}$ configuration contributes significantly to the 2_5^+ level. While the situation is reversed for the GXPF1A results, the overall agreement with the data is qualitatively the same and, in the absence of lifetime information, no further conclusion can be reached. At this point, it is, however, desirable to remember that the two interactions reverse the ordering of the two states of interest in the case of ^{55}Ti. In this instance, both β-decay data [37] and one-neutron knockout measurements at relativistic

energies [38] establish the ^{55}Ti ground state as $1/2^-$, with a $5/2^-$ excited level at 592 keV, in agreement with GXPF1A predictions.

It should be noted that the experimental position of the 10_2^+ state is markedly lower than any computed values. The closest calculated 10_2^+ state, obtained with the GXPF1A interaction, is overpredicted by 656 keV. The calculated dominant wave function component is associated with the $\pi f_{7/2}^2 \nu f_{7/2}^{-1} p_{3/2}^3$ configuration implying an excitation across the $N = 28$ gap. It would be of interest to locate additional levels in this regime of excitation energy and angular momentum to investigate further whether the interactions are unable to predict core breaking with a suitable degree of accuracy.

Finally, it is worth noting that none of the three effective interactions discussed here reproduces the measured g factors [29] for the 2_1^+ and 4_1^+ levels well. Specifically the computed values for the 2_1^+ g factors of 0.329, 0.292, and 0.355 obtained with the GXPF1A, KB3G, and FPD6 interactions, respectively, do not compare favorably with the measured value of 0.81(19) [29]. In the same way, the theoretical g factors of 1.032, 0.982, and 0.560 are in poor agreement with the measured value of 0.46(15) for the 4_1^+ state, with perhaps the exception of the FPD6 number. These discrepancies were remedied somewhat in Ref. [29] by a modification of the neutron single-particle energies. However, it is also possible that these discrepancies can be attributed to the lack of admixtures of small proton excitations into the state wave functions.

All in all, the comparisons between the data and the calculations appear to favor, to a degree, the results derived with the GXPF1A interaction. The single-particle energies and the matrix elements assumed with this Hamiltonian reproduces the presence of the $N = 32$ subshell gap in the Ti isotopic chain [10,12,14] and the absence of a similar gap at $N = 34$. The two other interactions reach the same conclusion. However, for the Ca isotopes, the predictions differ and the GXPF1A calculations still predict a 2_1^+ state at ∼3.0 MeV, ∼0.5 MeV higher than in ^{52}Ca, hereby implying the presence of a $N = 34$ gap in Ca. A similar conclusion was recently reached on the basis of comparisons between levels with dominant $\nu p_{3/2}^2 p_{1/2}$ and $\nu p_{3/2}^2 f_{5/2}$ configurations in ^{51}Ca [15].

V. CONCLUSIONS

Gamma-ray coincidence measurements using Gammasphere coupled with the FMA have provided detailed information on the yrast and non-yrast excitations in ^{52}Ti up to moderate spin. The spins and parities of the established levels were assigned based on measured transition multipolarities, intensity arguments and additional input from a complementary β-decay study. Lifetime information for some of the very short-lived states was obtained for the first time by determining the average velocities of the recoils at the points of decay inside the target. The extended ^{52}Ti level structure was compared with the results of shell-model calculations performed with the GXPF1A, FPD6, and KB3G interactions. The experimental data appear to be best described by the GXPF1A calculations. This observation is related to the relative ordering and energy spacing between the $\nu p_{3/2}$, $\nu p_{1/2}$, and $\nu f_{5/2}$ orbitals with the implication that the onset of a subshell closure at $N = 34$ in the Ca isotopes cannot yet be entirely ruled out.

ACKNOWLEDGMENTS

This work was supported by the US Department of Energy, Office of Nuclear Physics, under Contract No. DE-AC02-06CH11357, by the UK Science and Technology Facilities Council, by US National Science Foundation Grants No. PHY-01-01253, and PHY-0456463, and by Polish Scientific Committee Grant No. 2PO3B-074-18. A.N.D. acknowledges receipt of an STFC postdoctoral fellowship. The authors thank the ATLAS operating staff for the efficient running of the accelerator and John Greene for preparing the targets used in the measurement.

[1] J. I. Prisciandaro *et al.*, Phys. Lett. **B510**, 17 (2001).
[2] R. V. F. Janssens *et al.*, Phys. Lett. **B546**, 55 (2002).
[3] D. C. Dinca *et al.*, Phys. Rev. C **71**, 041302(R) (2005).
[4] A. Gade *et al.*, Phys. Rev. C **74**, 021302(R) (2006).
[5] A. Bürger *et al.*, Phys. Lett. **B622**, 29 (2005).
[6] T. Otsuka, R. Fujimoto, Y. Utsuno, B. A. Brown, M. Honma, and T. Mizusaki, Phys. Rev. Lett. **87**, 082502 (2001).
[7] P. F. Mantica *et al.*, Phys. Rev. C **67**, 014311 (2003).
[8] M. Honma, T. Otsuka, B. A. Brown, and T. Mizusaki, Phys. Rev. C **65**, 061301(R) (2002).
[9] B. Fornal *et al.*, Phys. Rev. C **72**, 044315 (2005).
[10] S. N. Liddick *et al.*, Phys. Rev. Lett. **92**, 072502 (2004).
[11] S. N. Liddick *et al.*, Phys. Rev. C **70**, 064303 (2004).
[12] B. Fornal *et al.*, Phys. Rev. C **70**, 064304 (2004).
[13] M. Honma, Eur. Phys. J. A **25**, suppl. 1, 499 (2005).
[14] S. Zhu *et al.*, Phys. Lett. **B650**, 135 (2007).
[15] B. Fornal *et al.*, Phys. Rev. C **77**, 014304 (2008).
[16] P. F. Mantica *et al.*, Phys. Rev. C **77**, 014313 (2008).
[17] R. A. Ricci and P. R. Maurenzig, Riv. Nuovo Cimento **1**, 291 (1969).
[18] M. Rejmund, S. Bhattacharyya, A. Navin, W. Mittig, L. Gaudefroy, M. Gelin, G. Mukherjee, F. Rejmund, P. Roussel-Chomaz, and C. Theisen, Phys. Rev. C **76**, 021304(R) (2007).
[19] S. J. Freeman *et al.*, Phys. Rev. C **69**, 064301 (2004).
[20] A. N. Deacon *et al.*, Phys. Lett. **B622**, 151 (2005).
[21] S. J. Freeman *et al.*, J. Phys. G: Nucl. Part. Phys. **31**, s1465 (2005).
[22] A. N. Deacon, Ph.D. thesis, University of Manchester (2006).
[23] S. Zhu *et al.*, Phys. Rev. C **74**, 064315 (2006).
[24] A. N. Deacon *et al.* (to be published).
[25] W. A. Richter, M. G. Van Der Merwe, R. E. Julies, and B. A. Brown, Nucl. Phys. **A523**, 325 (1991).
[26] A. Poves *et al.*, Nucl. Phys. **A694**, 157 (2001).
[27] J. F. Mateja, L. R. Medsker, C. P. Browne, J. D. Zumbro, H. T. Fortune, R. Middleton, and J. B. McGrory, Phys. Rev. C **23**, 2435 (1981).
[28] A. Huck, G. Klotz, A. Knipper, C. Miehe, C. Richard-Serre, G. Walter, A. Poves, H. L. Ravn, and G. Marguier, Phys. Rev. C **31**, 2226 (1985).

[29] K.-H. Speidel, J. Leske, S. Schielke, S. Bedi, O. Zell, P. Maier-Komor, S. Robinson, Y. Sharon, and L. Zamick, Phys. Lett. **B633**, 219 (2006).
[30] I. Y. Lee, Nucl. Phys. **A520**, 641c (1990).
[31] C. N. Davids, Nucl. Instrum. Methods Phys. Res. B **70**, 358 (1992).
[32] C. Jiang *et al.*, Nucl. Instrum. Methods Phys. Res. A **554**, 500 (2005).
[33] J. F. Ziegler, J. P. Biersack, and U. Littmark, *The Stopping and Range of Ions in Solids* (Pergamon Press, New York, 1985).
[34] J. Huo, S. Huo, and C. Ma, Nucl. Data Sheets **108**, 773 (2007).
[35] R. du Rietz *et al.*, Phys. Rev. Lett. **93**, 222501 (2004).
[36] M. Honma (to be published).
[37] P. F. Mantica *et al.*, Phys. Rev. C **68**, 044311 (2003).
[38] P. Maierbeck *et al.*, Phys. Lett. **B675**, 22 (2009).